ACS OMEGA

http://pubs.acs.org/journal/acsodf

Article

Insights into the Fracture Nature of Hematite from First Principles DFT Calculations

Hongliang Zhang, Wei Sun, Xian Xie, Jianyong He, and Chenyang Zhang*

Cite This: *ACS Omega* 2023, 8, 8248−8255

Read Online

ACCESS | Metrics & More | Article Recommendations | Supporting Information

ABSTRACT: Hematite, as an important iron source, usually crystallizes in the structure of rhombohedral R$\bar{3}$c in nature. To date, reports on the major exposed surface of hematite are still inconclusive. Herein, the fracture nature of hematite is studied by the density functional theory (DFT) method. The fracture surface morphology analysis predicts the fracture dominance of the (012) plane structurally. Besides, the lowest surface broken bond density (D_b) and the surface energy among all of the investigated surfaces also establish the exposure priority of the (012) surface. In addition, the (110) and (104) surfaces also show a strong fracture potential. In our proposed partition model, the exposure priority of (110) and (104) surfaces in region 2 with a lower surface energy and surface broken bond density is second only to the (012) surface. The other surfaces, except for the (012), (110), and (104) surfaces, are divided into region 3; here, the exposure of the surfaces located in this region is considered to be uncompetitive.

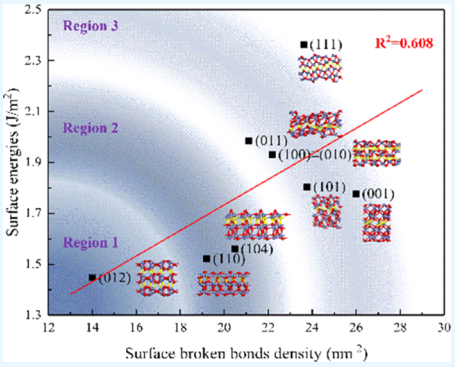

1. INTRODUCTION

Hematite, as an important iron source, usually crystallizes in the structure of rhombohedral R$\bar{3}$c in nature.[1] The enrichment and purification of hematite usually require a beneficiation treatment. Flotation, as one of the main beneficiation methods of hematite, usually achieves the separation of hematite from gangue minerals by selectively enhancing the difference in hydrophilicity and hydrophobicity of the mineral surface with the help of flotation reagents.[2,3] This determines that the realization of flotation involves a complex interface chemistry process. To accurately simulate the interfacial process, we usually need to identify the major fracture surface of a mineral.[4] However, the major fracture surface of hematite is still inconclusive.

The exposed surfaces of minerals generally include cleavage surfaces and fracture surfaces.[5,6] Generally speaking, the cleavage surface is usually the major exposed surface of minerals, while for minerals without a cleavage surface, the determination of the major exposed surface is quite difficult. Although the identification of commonly exposed surfaces in cleavage-free minerals is challenging, it does not mean we have no solution. It has been reported that there is anisotropy in the fracture of mineral planes, and this fracture anisotropy makes crystal planes show different exposure abilities.[7,8] Interestingly, the anisotropy of mineral crystals also shows the chargeability difference of the different exposed surfaces, and there is a significant correlation between the reactivity of mineral surfaces and their chargeability.[9,10] In addition, the anisotropy of a mineral surface also plays an important role in the adsorption priority of flotation reagents. For diaspores, the adsorption of oleate on the (001) surface is easier than that on the (010) surface, while the adsorption of oleate on the (001) surface is much less than that on the (110) surface for kaolinite.[11] Such a discrepancy in the result indicates that erroneous results will be obtained if the major exposed surface of minerals cannot be well determined when studying the flotation separation mechanism of minerals.

To evaluate the cleavage/fracture difficulty of mineral crystals, Gao successively proposed theories such as the surface broken bond density (D_b)[12,13] and crystal surface fracture energy (S_c)[14,15] and pointed out that for minerals with only one type of fracture bond, the S_c is positively correlated with D_b. At present, the D_b method has been successfully applied to predict the major exposed surfaces of various minerals and analyze the reactivity of different surfaces. Song et al.[16] found that the (112) surface with a smaller broken bond density is more likely to be broken than the (001) surface, thereby explaining the cleavage characteristics and exposed surface properties of wulfenite. Wang et al.[17] studied the crystal anisotropy and mineral surface activity difference of smithsonite, calcite, and dolomite by means of the D_b method, which provides a basis for the screening of high-efficiency reagents. Zhu et al.[18] analyzed the reactivity of different crystal planes of spodumene with the help of the D_b method. Similar

Received: September 21, 2022
Accepted: December 2, 2022
Published: February 21, 2023

application of the D_b method is also reflected in the adsorption behaviors of the anionic collector on the different surfaces of cassiterite studied by Wu et al.[19]

Surface energy is another method commonly used to characterize surface reactivity and the surface fracture possibility.[20] It is generally believed that the lower the surface energy, the higher the stability of the crystal face and the greater the fracture probability.[21] Gao et al.[8] found that there is a good linear correlation between surface energy and surface broken bond density, and the general rule is that the smaller the surface energy, the smaller the surface broken bond density. Some pieces of evidence have shown that this law generally exists in sulfide minerals (such as pyrite, sphalerite), oxide minerals (such as cassiterite, rutile, and anatase), and salt-type minerals (barite).[22]

For hematite, Gao et al.[22] believed that (012) and (104) were the major exposed surfaces, which is consistent with the report of Guo et al.,[23] who observed clear lattice fringes of hematite nanoparticles with a dihedral angle of 86° by a high-resolution transmission electron microscope (HR-TEM), thus confirming the dominant position of the hematite (012) surface. However, Yuan et al.[24] predicted that (110), (101), and (011) were the main fracture surfaces of hematite from the perspective of mechanical properties. In addition, it is reported that the Fe-terminated surface of the (001) plane is also considered a potential exposed surface.[25−28]

As mentioned, tremendous efforts have been made to determine the commonly exposed surfaces of hematite through experimental characterizations and theoretical calculations. It is puzzling that these reports draw different conclusions, due to which it will be difficult for us to determine which plane is the major exposed surface for hematite. Herein, the main objective of this fundamental research is to systematically investigate the exposure ability of seven low-index surfaces and two reported surfaces (012 and 104) of hematite through fracture surface morphology, surface energy, and surface broken bonds density to determine the major exposed surfaces of the hematite crystal and provide guidance for subsequent interface adsorption simulation.

2. COMPUTATIONAL METHODS AND MODELS

2.1. Computational Details. The density functional theory (DFT) calculations for hematite models were calculated using the CASTEP module in Materials Studio 2017. In the calculations, the exchange-correlation potential was modeled using generalized gradient approximation (GGA) parameterized by Perdew, Burke, and Ernzerhof (PBE).[29] The interaction between ion cores and valence electrons was described by Ultrasoft pseudopotentials, and the valence electron configurations Fe $3d^6 4s^2$ and O $2s^2 2p^4$ were performed. Owing to the strong electron correlations of Fe series oxides, the effective Coulomb repulsion parameter U was set as 4.2 eV for 3d electronic states of Fe atoms of hematite with an antiferromagnetic ordering.[25,30] The energy cutoff of the plane wave was set as 380 eV.[2] For self-consistent field iteration, the Pulay density mixing method was employed with a convergence tolerance of 2.0×10^{-6} eV/atom. The convergence-tolerance values of energy, maximum force, maximum stress, and maximum displacement were set as 2.0×10^{-5} eV/atom, 0.05 eV/Å, 0.1 GPa, and 0.002 Å, respectively.

2.2. Surface Energy, Surface Broken Bond Density, and Crystal Surface Fracture Energy. Surface energy (γ) is a measure to characterize the thermodynamic stability of surfaces, with a low value indicating a stable and fragile surface.[31] The surface energy can be calculated as follows[32]

$$\gamma = \frac{E_s - N \times E_{bulk}}{2 \times A} \quad (1)$$

where E_s and E_{bulk} are the energies of the surface model and the bulk cell, respectively, N is the formula units contained in the surface model, and A is the surface area.

Surface broken bond density (D_b) defined by Gao et al. is calculated by the following formula[8]

$$D_b = N_b/A \quad (2)$$

where D_b is the broken bond number per nm2, and N_b and A are the broken bond number and surface area of the slab model, respectively.

The crystal surface fracture energy (S_c) is the ratio of the sum of the fracture bond energies of various types of chemical bonds on the crystal surface to the area of the corresponding fracture plane. The S_c can be calculated as follows[14]

$$S_c = \frac{\sum_{i=1}^{n} N_{b(i)} \times E_{(i)}}{A} \quad (3)$$

where $N_{b(i)}$ is the number of identical bonds i broken in a specific crystal surface, n is the type of fracture bond, and $E_{(i)}$ is the fracture energy of bond i.

3. RESULTS AND DISCUSSION

3.1. Bulk Cell and Slab Models. The bulk cell structure of hematite in ref 33 was introduced as the initial structure for hematite. The lattice parameters of the bulk cell are $a = b =$ 5.0355 Å and $c =$ 13.7471 Å. In structure optimization calculations, the Brillouin zone mesh was sampled with $5 \times 5 \times 2$ for the bulk cell. The optimized bulk cell structure is shown in Figure 1a; compared with experimental lattice parameters of the initial structure, the largest discrepancy was only 2.54%,

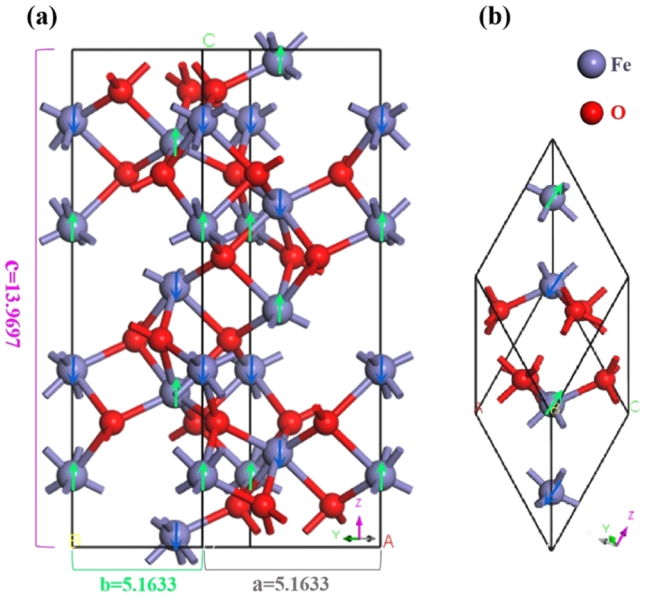

Figure 1. Crystal structure of hematite: (a) optimized structure of the hematite bulk cell, (b) rhombohedral unit cell of the optimized bulk cell. Arrows represent the orientation of magnetic moments in the antiferromagnetic alignment.

https://doi.org/10.1021/acsomega.2c06101
ACS Omega 2023, 8, 8248−8255

Table 1. Brillouin Zone Mesh, Surface Area, and Broken Bond Number (N_b) for Slab Models of Hematite

slab models	formula units (n)	lattice parameters			surface area (nm^2)	Brillouin zone mesh	$N_{b(tot)}$	$N_{b(\alpha)}$	$N_{b(\beta)}$
		a (nm)	b (nm)	c (nm)					
(001)	4	1.0327	1.0327	3.3324	0.9235	3 × 3 × 1	24	0	24
(010)	4	1.3970	1.0327	2.7702	1.4426	2 × 3 × 1	32	16	16
(011)	4	1.0327	1.4893	2.8321	1.5147	3 × 2 × 1	32	16	16
(012)	4	1.0327	1.1058	2.9833	1.1419	3 × 3 × 1	16	16	0
(100)	4	1.0327	1.3970	2.7702	1.4426	3 × 2 × 1	32	16	16
(101)	4	1.1058	1.0327	3.2304	1.0098	3 × 3 × 1	24	8	16
(104)	4	1.5130	1.0327	2.7849	1.5624	2 × 3 × 1	32	16	16
(110)	4	1.5130	1.1058	2.7172	1.6658	2 × 3 × 1	32	16	16
(111)	4	0.8943	1.4893	3.0037	1.2705	3 × 2 × 1	30	15	15

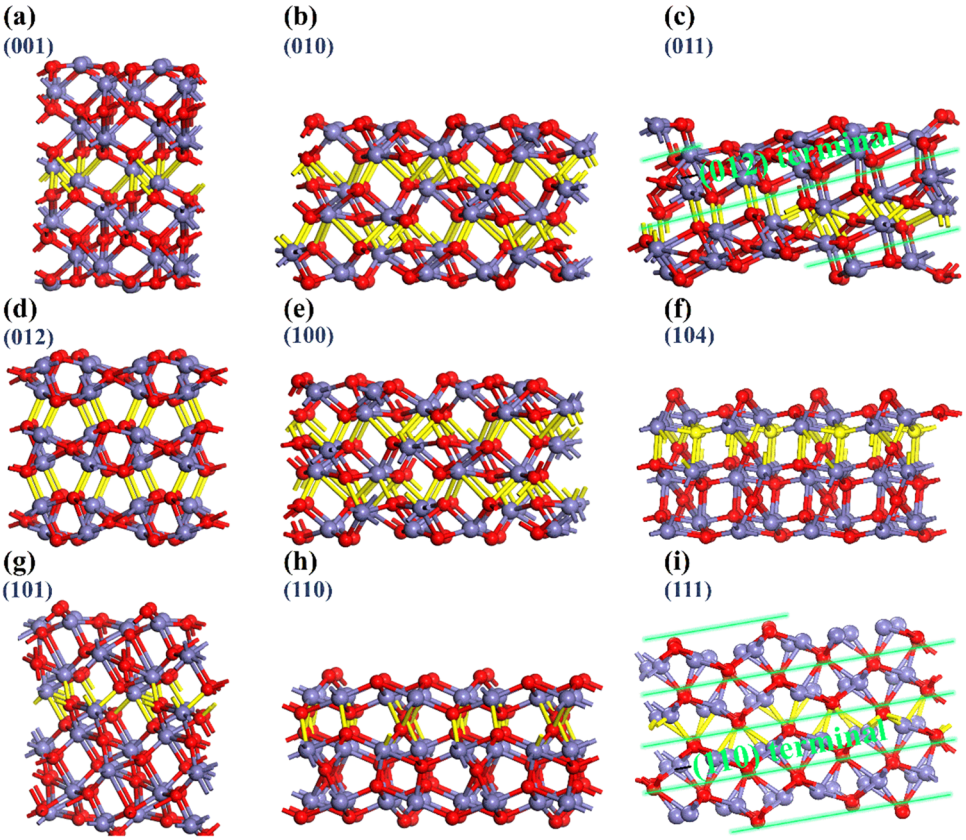

Figure 2. Optimized surface models of hematite: (a) hematite (001) surface, (b) hematite (010) surface, (c) hematite (011) surface, (d) hematite (012) surface, (e) hematite (100) surface, (f) hematite (104) surface, (g) hematite (101) surface, (h) hematite (110) surface, and (i) hematite (111) surface.

which indicated that the optimized structure was reasonable since the discrepancy was within the acceptable error value of 5%.[34] Figure 1b is the primitive cell of the optimized bulk cell structure in Figure 1a, and it clearly reflects the antiferromagnetic arrangement of the bulk cell in Figure 1a.

The slab models of hematite were cleaved from the optimized bulk cell structure in Figure 1a. The periodicity of the crystal was retained during the construction process of the slab models, and all of the constructed slab models were kept neutral and stoichiometric to avoid polarizing electric fields.[35] The symmetries of the top and bottom surfaces of the surface model were fully considered while cleaving the surface. If the atomic arrangement of the crystal structure does not allow symmetry to be obtained for a particular surface, the cleaved surface with the minimum density of broken bonds will be considered. Based on the above-mentioned constraints, we constructed nine surfaces of hematite, including seven low-index surfaces, and two surfaces reported by Gao et al., who believe that the (104) and (012) surfaces were the commonly exposed surfaces of hematite particles.[22] Finally, the surface models with 20 Å vacuum thickness and 7−14 Å slab thickness were constructed, and the corresponding lattice parameters, surface area, broken bond number, and k-point mesh for the surface calculations are listed in Table 1.

3.2. Fracture Surface Morphology Analysis. The optimized optimal fracture planes of surfaces of hematite in Table S1 are presented in Figure 2, and the broken bonds generated on the surfaces during the surface cleaving process are displayed in yellow. The (010) ≡ (100) and (012) have obvious layered structures, which indicates that the (010) ≡ (100) and (012) planes are most likely to be the major exposed surfaces or cleavage surfaces of hematite. The

https://doi.org/10.1021/acsomega.2c06101
ACS Omega 2023, 8, 8248−8255

Table 2. Surface Broken Bond Density (nm^{-2}) for Slab Models of Hematite

references	(001)	(010)	(011)	(012)	(100)	(101)	(104)	(110)	(111)
this work	25.99	22.18	21.13	14.01	22.18	23.77	20.48	19.21	23.61
ref 22	27.30			14.61		24.97	21.43	19.91	

interlayer spacing (vertical distance between the bonding atoms Fe and O) of the above three surfaces with layered structures of hematite are 1.50 and 1.73 Å, respectively, and the spacing of the (012) surface is 0.23 Å larger than that of the (010) ≡ (100) surfaces. From the results of the interlayer spacing, the (012) surface is easier to expose than the (010) ≡ (100) surfaces. In addition, the (110) surface is also expected to be a commonly exposed surface of hematite due to the electrostatic repulsion between the adjacent O^{2-} layers. For (001), (101), (011), and (111) surfaces, the exposure probability may be weak due to the disordered arrangement of Fe and O atoms spatially. In addition, the exposure of the (011) surface needs to cleave the (012) orientation obliquely, which also reflects the difficulty of its exposure. In summary, the special layered structures of the (012), (010) ≡ (100) and (110) surfaces show strong exposure potential to a certain extent, but this exposure potential is not reflected on other surfaces.

3.3. Surface Broken Bond Density. To further explore the exposure ability of each plane of hematite, here, we made statistics on the density of broken bonds on the surfaces of hematite. The broken bond number and the surface area of the surfaces in Figure 2 are listed Table 1. The calculated surface broken bond densities of fracture surfaces are listed Table 2. The broken bond density of the fracture surfaces follows the order (001) > (101) > (111) > (010) ≡ (100) > (011) > (104) > (110) > (012), which is consistent with the research results of Gao et al.,[22] who investigated five fracture surfaces of hematite, and the broken bond density of the fracture surfaces has the following order: (001) > (101) > (104) > (110) > (012). The above results show that the surface broken bond density with a value of 25.99 nm^{-2} on the (001) plane is the largest among all of the investigated surfaces, which indicates that the exposure of (001) planes is not conducive, and the strong electrostatic interaction between the alternately arranged Fe^{3+} layers and O^{2-} layers along the (001) surface also prevents the fracture of the (001) planes. In addition, from the perspective of crystal growth, hematite particles have strong crystal plane selectivity in the process of mutual aggregation and consolidation. Generally, the oriented attachment of $(001)_{hcp}$ // $(001)_{hcp}$ and $(001)_{hcp}$//$(101)_{hcp}$ orientations are regarded as two major growth mechanisms.[22,36] The growth surfaces of the crystal usually have high activity, so it is not realistic for hematite to fracture on (001) and (101) planes. For the (010) ≡ (100) and (012) planes with the layered structures in Figure 2, the (012) surface has the lowest surface broken bond density with a value of 14.01 nm^{-2}. In addition, the interlayer spacing of the (012) surface is larger than that of (010) ≡ (100) surfaces. In this case, the (012) surface with a low broken bond density and a large interlayer spacing can be regarded as a commonly exposed surface of hematite particles. In addition, the (110) and (104) surfaces with surface broken bond densities of 19.21 and 20.48 nm^{-2} also show a strong exposure ability.

3.4. Crystal Surface Fracture Energy. In hematite, the central Fe atom is coordinated with six O atoms, and its structure is shown in Figure 3. The FeO_6 coordination

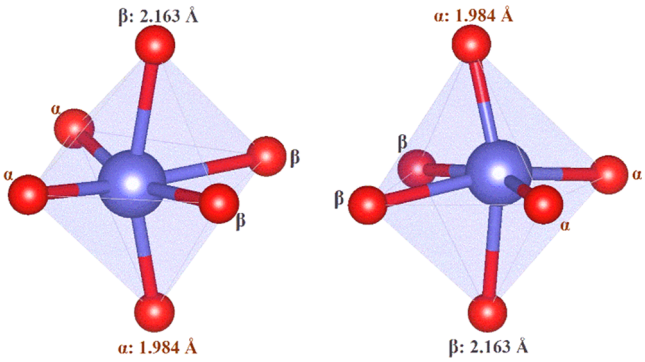

Figure 3. Coordination structure of the central Fe atom in the optimized hematite crystal.

structure shows an irregular octahedral structure, so its Fe−O bonds are not completely equivalent. The bond lengths between the mirror symmetrical O atoms and the central Fe atom are 1.984 and 2.163 Å, respectively; here, we mark them as bond α and bond β.

Fracture energy is an important parameter to measure the strength of chemical bonds. However, there is currently no method to directly calculate the fracture energy of chemical bonds in crystals. Gao et al.[14] proposed a weighted bond energy according to the bond order to approximate the fracture energy. Here, we adopt a cluster model with H atoms (FeO_6H_{12}) configured to approximate the fracture energy of the Fe−O bonds shown in Figure 4. In geometric optimization, the Fe−O frameworks FeO_6 and FeO_5 of FeO_6H_{12} and FeO_5H_{10} clusters are constrained. The calculated fracture energies of the α-bond and β-bond are 296.69 and 252.12 kJ/mol, respectively. On this basis, we further obtain the surface fracture energy of the specific crystal plane of hematite according to formula 3. The crystal surface fracture energy of hematite surfaces is shown in Table 3. This result shows that the (012) surface possesses a significantly lower surface fracture energy than the other surfaces, implying that the (012) surface is the preferentially exposed surface of hematite. Second, the (110) and (104) planes with surface fracture energies of 4.39 and 4.68 J/m^2 are also preliminarily predicted to be the major exposed surfaces of hematite. For surfaces other than (012), (110), and (104), the larger surface fracture energies would prevent their exposure.

Figure 5 shows that there is a good linear relationship between the surface fracture energy and the surface broken bond density; the corresponding coefficient of determination R^2 is 0.973. Such a result indicates that the difference of Fe−O bonds in hematite has little effect on the fracture properties of each crystal plane of hematite. The main reason is that the numbers of fractures of the α-bond and the β-bond on most surfaces of hematite are equally distributed, and second, the fracture energy difference between bond α and bond β is small, which is not enough to cause the surface fracture energy of some surfaces to seriously deviate from the fitting line.

3.5. Surface Energy. Surface energy helps understand the surface stability and exposure performance of minerals, and the

https://doi.org/10.1021/acsomega.2c06101
ACS Omega 2023, 8, 8248−8255

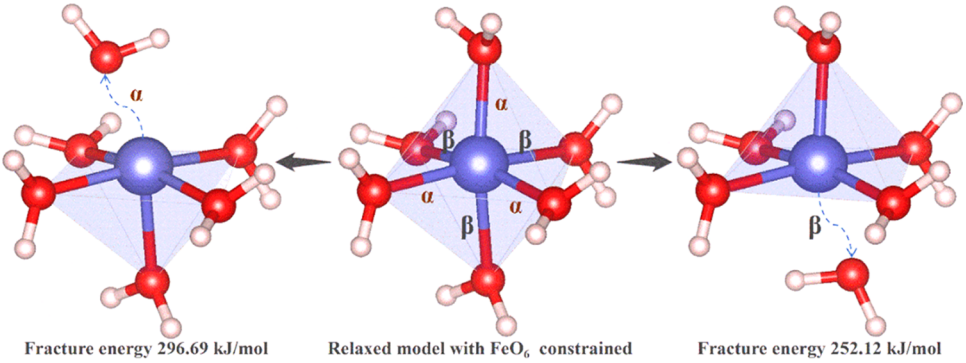

Figure 4. Constraint optimization of the models for α-bond and β-bond fracturing while keeping the Fe−O frameworks unchanged.

Table 3. Crystal Surface Fracture Energies (J/m^2) of the Hematite Surfaces

surfaces	(001)	(100)≡(010)	(011)	(012)	(101)	(104)	(110)	(111)
S_c	5.46	5.07	4.83	3.46	5.29	4.68	4.39	5.40

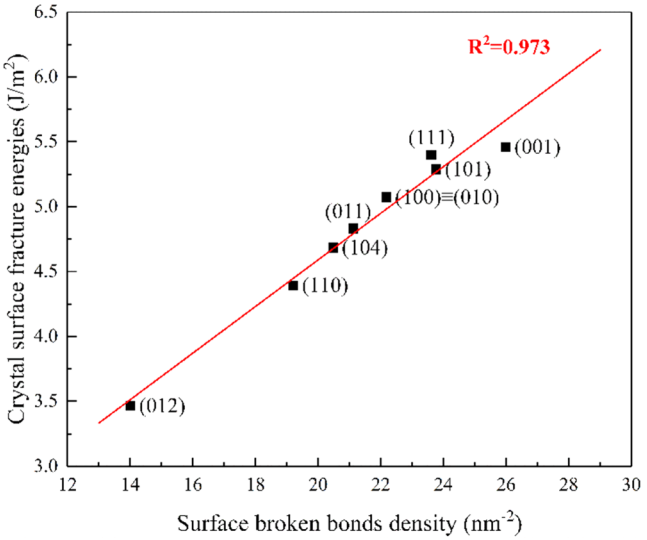

Figure 5. Linear fitting correlation analysis plot of crystal surface fracture energy and surface broken bond density.

calculation of surface energy requires the total energy of the mineral surface model. The surface energies of the optimal fracture termination of the surfaces for hematite are recorded in Table S2. The results show that the surface energies of the surfaces with and without dispersion correction show a good linear relationship (R^2 is 0.991 as shown in Figure S1). Given the consistency with previous works,[2,30] the results without dispersion correction were used for subsequent analysis.

The surface energies for the relaxed and unrelaxed slab models of hematite are listed in Table 4. The results show that the surface energies of the optimized surface structures are generally decreased, which indicates that the stability of the surface structures after geometry optimization is improved. Considering that the surface energies of the unrelaxed surfaces can better reflect the strength of the destruction of intermolecular chemical bonds at the moment of creating the surface, the evaluation of the surface fracture ability should be based on the surface energy of the unrelaxed surface structure. The surface energies of the unrelaxed surfaces listed in Table 4 follow the order (012) < (110) < (104) < (001) < (101) < (100) ≡ (010) < (011) < (111). Among them, the surface energy of the (111) surface with a value of 2.36 J/m^2 is much larger than that of the other investigated surfaces, indicating that it is difficult to expose the (111) surfaces of hematite. It is worth noting that the exposure of the (111) obliquely truncated (110) plane does present great difficulties. The (011) surface with a surface energy of 2.08 J/m^2 ranks second below the (111) surface, while the surface energy of the (011) surface is the largest among all of the low-index surfaces investigated by de Leeuw and Cooper,[20] which indicates that the exposure of the (011) surface is thermodynamically unfavorable. In addition, it is also a challenge to obliquely cleave the plate-like structure of the (012) surface to achieve the exposure of the (011) surface due to the special crystal structure of hematite. For the (010) ≡ (100) surfaces, although they have the same layered structure as the goethite (010) perfect cleavage surface, the larger surface fracture bond density (22.18 nm^{-2}) and the moderately strong surface energy (1.91 J/m^2) hinder the exposure of the hematite (010) ≡ (100) surfaces. The (101) surface with a surface energy of 1.80 J/m^2 ranks fourth next to (010) ≡ (100) surfaces. The atomic arrangement without the layered structure makes the (101) surface impossible to be a cleavage plane of hematite, which indicated that the exposure for the hematite (101) surface is difficult. For the (001) surface, due to the high coordination unsaturation of Fe atoms on the surface, the coordination field of the surface Fe atoms will be distorted during the optimization process to show a lower surface energy. Therefore, the surface energy is not enough to judge the exposure ability for the (001) surface. Here, we believe that the

Table 4. Surface Energies (J/m^2) for the Relaxed and Unrelaxed Slab Models of Hematite

state	references	(001)	(100)≡(010)	(011)	(012)	(101)	(104)	(110)	(111)
relaxed	this work	0.92	1.11	1.20	1.07	1.19	1.10	1.05	1.51
unrelaxed	this work	1.78	1.91	2.08	1.41	1.80	1.56	1.52	2.36
	20	1.78	1.99	2.41	1.88	2.34		2.03	2.07

https://doi.org/10.1021/acsomega.2c06101
ACS Omega 2023, 8, 8248−8255

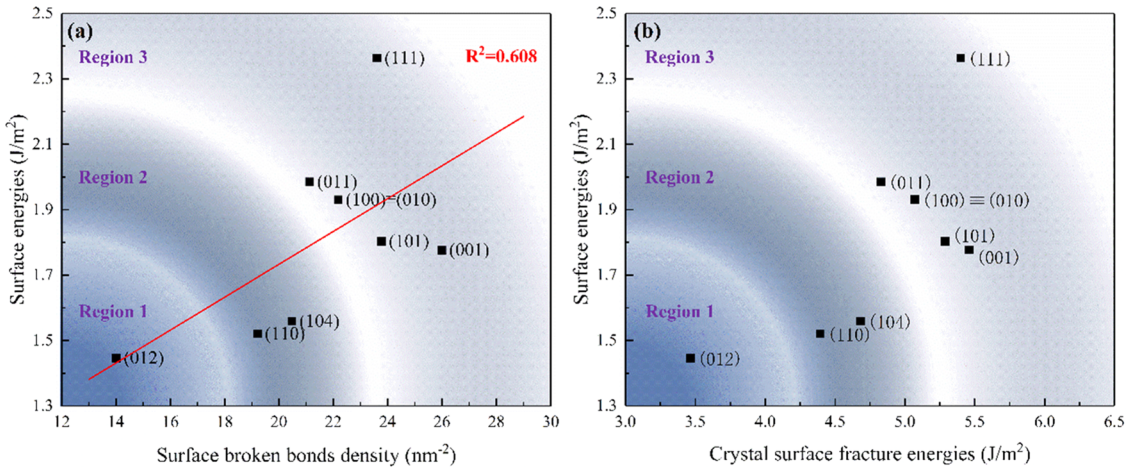

Figure 6. Two-dimensional models: (a) relationship between the surface energy and surface broken bond density, and (b) relationship between the surface energy and crystal surface fracture energy.

exposure of the (001) surface is difficult from the perspective of the surface broken bond density and the orientation of crystalline growth.[22,36] The (110) surface has been reported to be a possible exposed surface of hematite.[37,38] The atomic arrangement of the (110) surface is constructed by the alternating −Fe−O−O− unit layers, which makes the (110) surface easy to fracture due to the electrostatic repulsion of the adjacent O layers. In addition, lower surface energy (1.52 J/m^2) and surface broken bond density (19.21 nm^{-2}) are also favorable for the exposure parallel to the (110) plane. For the (104) surface, the surface broken bond density and the surface energy are very close to the (110) surface, which to some extent recognizes the exposure of the (104) surface, and previous studies also tend to identify the exposure of the (104) surface for isomorphous ilmenite-hematite series.[21,22,39−41] Besides, the (012) surface with a layered structure is also predicted to be a major exposed surface of hematite due to its extremely low broken band density (14.01 m^{-2}) and surface energy (1.07 J/m^2), and the exposure ability of the (012) surface is better than that of (110) and (104) surfaces. In addition, HR-TEM also confirmed the extensive exposure of the (012) surface in the hematite particles.[23]

3.6. Two-Dimensional Model for Assessing the Hematite Fracture Nature. The two-dimensional model of the relationship between surface energy and surface broken bond density is drawn in Figure 6a. It can be seen that the surface energies and surface broken bond density of the surfaces showed a bad linear relationship, and the coefficient of determination R^2 is 0.608. It is particularly noteworthy that all surfaces except for (012) and (010) ≡ (100) surfaces show strong discreteness. Therefore, separate analysis of the surface fracture bond density or surface energy is not enough to accurately evaluate the fracture performance of each crystal plane of hematite.

Here, to more intuitively and accurately evaluate the exposure ability of the hematite surfaces, we subdivide the fracture ability of each surface of hematite into three regions. The surface in region 1 with a low fracture bond density and surface energy is the most ideal exposed surface of hematite, and only the (012) surface exists in this region. The surfaces in region 3 possess a high surface energy, or high fracture bond density, or both. The exposure ability of the surfaces in this region is significantly weaker than that in region 1. Most of the crystal surfaces of hematite are located in this area, which shows their poor exposure ability. The surfaces in region 2 possess a moderate level of surface energy or surface broken bond density, the exposure ability of surfaces (110) and (104) in this region is weaker than that of region 1 but advantageous to that of region 3. In summary, the exposure ability of the seven surfaces in region 3 is relatively difficult. The major exposed surfaces of hematite should be the (012) surface in region 1 and the (110) and (104) surfaces in region 2, and the exposure ability of the (012) surface is superior to that of the (110) and (104) surfaces. Figure 6b shows the relationship between the surface energy and the crystal surface fracture energy. Due to the crystal surface, the fracture energy shows a good linear relationship with the surface broken bond density; in the two-dimensional model of Figure 6b, the region where each crystal plane is located is consistent with that of Figure 6a, which suggests the exposure priority of the (012), (110), and (104) surfaces. To summarize, we have reason to believe that the major exposed surfaces of hematite are (012), (110), and (104) surfaces.

4. CONCLUSIONS

In this work, the exposure abilities of seven low-index surfaces and two reported potentially exposed surfaces of hematite were predicted by fracture surface morphology analysis, surface broken bond density, and surface energy based on DFT calculations. The fracture surface morphology analysis preliminarily determined that the (012) surface with large interlayer spacing and the (110) surface with strong electrostatic repulsion of the adjacent O^{2-} layers have obvious fracture superiority. This fracture superiority is also reflected in the surface broken bond density and surface energy. The (012) surface with a special layered structure has the lowest surface broken bond density and surface energy among all surfaces, which establishes its priority in fracture. In addition, the (110) and (104) planes with a relatively low surface energy and surface fracture bond density are also predicted to be the major fracture planes of hematite. They are located in region 2 in our proposed hematite fracture model, and the exposure priority is second only to the (012) surface. Surfaces other than (012), (110), and (104) possess a high surface energy or a high surface broken bond density, or both, which determines that their exposure probability is very low.

https://doi.org/10.1021/acsomega.2c06101
ACS Omega 2023, 8, 8248−8255

■ ASSOCIATED CONTENT

Supporting Information

The Supporting Information is available free of charge at https://pubs.acs.org/doi/10.1021/acsomega.2c06101.

Surface broken bond number and energies of surfaces with different terminating planes; surface energies of the optimal fracture planes of surfaces with and without dispersion; and linear fitting correlation analysis plot of surface energies with and without dispersion corrections (PDF)

■ AUTHOR INFORMATION

Corresponding Author

Chenyang Zhang − *School of Minerals Processing and Bioengineering, Central South University, Changsha 410083, China; State Key Laboratory of Complex Nonferrous Metal Resources Clean Utilization, Kunming University of Science and Technology, Kunming 650093, China; Key Laboratory of Hunan Province for Comprehensive Utilization of Complex Copper-Lead Zinc Associated Metal Resources, Hunan Research Institute for Nonferrous Metals, Changsha 410100, China;* orcid.org/0000-0002-5806-2605; Email: zhangchenyang@csu.edu.cn

Authors

Hongliang Zhang − *School of Minerals Processing and Bioengineering, Central South University, Changsha 410083, China;* orcid.org/0000-0002-4338-7263

Wei Sun − *School of Minerals Processing and Bioengineering, Central South University, Changsha 410083, China;* orcid.org/0000-0002-0204-4520

Xian Xie − *State Key Laboratory of Complex Nonferrous Metal Resources Clean Utilization, Kunming University of Science and Technology, Kunming 650093, China*

Jianyong He − *School of Minerals Processing and Bioengineering, Central South University, Changsha 410083, China;* orcid.org/0000-0002-6903-5987

Complete contact information is available at: https://pubs.acs.org/10.1021/acsomega.2c06101

Author Contributions

H.Z.: Writing—original draft, formal analysis, conceptualization, methodology, software, writing—review and editing. W.S.: Formal analysis, software, writing—review and editing. X.X.: Visualization, writing—review and editing, validation. J.H.: Investigation, data curation, writing—review and editing. C.Z.: Supervision, methodology, funding acquisition, writing—review and editing.

Notes

The authors declare no competing financial interest.

■ ACKNOWLEDGMENTS

This work was financially supported by the National Key Research and Development Program of China (No. 2019YFC0408303), the Natural Science Foundation of China (Nos. 52074356, U20A20269), the Natural Science Foundation of Hunan Province (Nos. 2021JJ20069, 2020JJ5759); the China Postdoctoral Science Foundation (Nos. 2020T130188, 2018M642988), the Changsha Outstanding Innovative Youth Training Program (No. kq2009005), and the Higher Education Discipline Innovation Project, 111 Project (No. B14034). This work was carried out in part using hardware and/or software provided by a Tianhe II supercomputer at the National Supercomputing Center in Guangzhou and the High Performance Computing Centers of Central South University and Nanjing University.

■ REFERENCES

(1) Hill, A. H.; Jiao, F.; Bruce, P. G.; Harrison, A.; Kockelmann, W.; Ritter, C. Neutron diffraction study of mesoporous and bulk hematite, alpha-Fe2O3. *Chem. Mater.* **2008**, *20*, 4891−4899.

(2) Zhang, H.; Xu, Z.; Sun, W.; Chen, D.; Li, S.; Han, M.; Yu, H.; Zhang, C. Selective adsorption mechanism of dodecylamine on the hydrated surface of hematite and quartz. *Sep. Purif. Technol.* **2021**, *275*, No. 119137.

(3) Zhang, H.; Zhang, F.; Sun, W.; Chen, D.; Chen, J.; Wang, R.; Han, M.; Zhang, C. The effects of hydroxyl on selective separation of chalcopyrite from pyrite: A mechanism study. *Appl. Surf. Sci.* **2023**, *608*, No. 154963.

(4) Zhang, H.; Sun, W.; Zhu, Y.; He, J.; Chen, D.; Zhang, C. Effects of the Goethite Surface Hydration Microstructure on the Adsorption of the Collectors Dodecylamine and Sodium Oleate. *Langmuir* **2021**, *37*, 10052−10060.

(5) Gao, Z.; Li, C.; Sun, W.; Hu, Y. Anisotropic surface properties of calcite: A consideration of surface broken bonds. *Colloids Surf., A* **2017**, *520*, 53−61.

(6) Geng, Y.; Xu, D.; Wang, X.; Yu, G.; Zhang, G.; Zhang, H. AFM study of surface morphology of {100} cleavage planes of L-arginine acetate crystals. *J. Cryst. Growth* **2005**, *282*, 208−213.

(7) Ebrahimi, F.; Kalwani, L. Fracture anisotropy in silicon single crystal. *Mat. Sci. Eng. A* **1999**, *268*, 116−126.

(8) GAO, Z.-y.; Sun, W.; Hu, Y.; Liu, X. Anisotropic surface broken bond properties and wettability of calcite and fluorite crystals. *Trans. Nonferrous Met. Soc. China* **2012**, *22*, 1203−1208.

(9) Gao, Z.; Hu, Y.; Sun, W.; Drelich, J. W. Surface-Charge Anisotropy of Scheelite Crystals. *Langmuir* **2016**, *32*, 6282−6288.

(10) Gao, Z.; Xie, L.; Cui, X.; Hu, Y.; Sun, W.; Zeng, H. Probing Anisotropic Surface Properties and Surface Forces of Fluorite Crystals. *Langmuir* **2018**, *34*, 2511−2521.

(11) Xu, L.; Hu, Y.; Dong, F.; Gao, Z.; Wu, H.; Wang, Z. Anisotropic adsorption of oleate on diaspore and kaolinite crystals: Implications for their flotation separation. *Appl. Surf. Sci.* **2014**, *321*, 331−338.

(12) Gao, Z.; Fan, R.; Ralston, J.; Sun, W.; Hu, Y. Surface broken bonds: An efficient way to assess the surface behaviour of fluorite. *Miner. Eng.* **2019**, *130*, 15−23.

(13) Hu, Y.; Gao, Z.; Sun, W.; Liu, X. Anisotropic surface energies and adsorption behaviors of scheelite crystal. *Colloids Surf., A.* **2012**, *415*, 439−448.

(14) He, J.; Wu, Y.; Sun, W.; Gao, Z. Crystal plane fracture energy and its fracture mechanism: A case study of zircon. *Chin. J. of Nonferrous Met.* **2021**, 1−18.

(15) Gao, Z.*Investigation On the Relationship Between Anisotropic Crystal Surface Characteristics and Flotation Behaviors of Three Calcium-Bearing Minerals*; Central South University: Changsha, 2013.

(16) Song, B.; Tao, D.; Li, P.; Wang, X.; Ran, J. Cleavage nature and surface appearances of wulfenite by first-principles calculations and experimental measurement. *Results Phys.* **2020**, *16*, No. 102849.

(17) Wang, J.; Sun, Z.; Bai, J. Research on Crystal Anisotropy and Surface Properties of Smithsonite. *Conserv. Util. Miner. Resour.* **2021**, *41*, 1−6.

(18) Zhu, G.; Wang, Y.; Liu, X.; Yu, F.; Lu, D. The cleavage and surface properties of wet and dry ground spodumene and their flotation behavior. *Appl. Surf. Sci.* **2015**, *357*, 333−339.

(19) Wu, H.; Renno, A. D.; Foucaud, Y.; Rudolph, M. Study of the Influence of the Crystallographic Orientation of Cassiterite Observed with Colloidal Probe Atomic Force Microscopy and its Implications for Hydrophobization by an Anionic Flotation Collector. *ACS Omega* **2021**, *6*, 4212−4226.

(20) de Leeuw, N. H.; Cooper, T. G. Surface simulation studies of the hydration of white rust Fe(OH)(2), goethite alpha-FeO(OH) and hematite alpha-Fe2O3. *Geochim. Cosmochim. Acta* **2007**, *71*, 1655−1673.
(21) Li, L.; Zhang, C.; Yuan, Z.; Liu, Z.; Li, C. Selectivity of Benzyl Hydroxamic Acid in the Flotation of Ilmenite. *Front. Chem.* **2019**, *7*, No. 886.
(22) Gao, Z.-y.; Sun, W.; Hu, Y.-h. Mineral cleavage nature and surface energy: Anisotropic surface broken bonds consideration. *Trans. Nonferrous Met. Soc. China* **2014**, *24*, 2930−2937.
(23) Guo, S.-q.; Hu, Z.; Zhen, M.; Gu, B.; Shen, B.; Dong, F. Insights for optimum cation defects in photocatalysis: A case study of hematite nanostructures. *Appl. Catal., B* **2020**, *264*, No. 118506.
(24) Yuan, Z.; Zhang, C.; Li, L.; Xu, X.; Wang, X. Density functional theory calculation of fracture surfaces of siderite and hematite. *Powder Technol.* **2020**, *376*, 373−379.
(25) Nguyen, M.-T.; Seriani, N.; Gebauer, R. Water adsorption and dissociation on alpha-Fe2O3(0001): PBE+U calculations. *J. Chem. Phys.* **2013**, *138*, No. 194709.
(26) Pang, Q.; DorMohammadi, H.; Isgor, O. B.; Árnadóttir, L. Density functional theory study on the effect of OH and Cl adsorption on the surface structure of alpha-Fe2O3. *Comput. Theor. Chem.* **2017**, *1100*, 91−101.
(27) Song, Z.; Wang, B.; Yu, J.; Ma, C.; Zhou, C.; Chen, T.; Yan, Q.; Wang, K.; Sun, L. Density functional study on the heterogeneous oxidation of NO over alpha-Fe2O3 catalyst by H2O2: Effect of oxygen vacancy. *Appl. Surf. Sci.* **2017**, *413*, 292−301.
(28) Wang, R. B.; Hellman, A. Surface terminations of hematite (alpha-Fe2O3) exposed to oxygen, hydrogen, or water: dependence on the density functional theory methodology. *J. Phys.: Condens. Matter* **2018**, *30*, No. 275002.
(29) Perdew, J. P.; Burke, K.; Ernzerhof, M. Generalized Gradient Approximation Made Simple. *Phys. Rev. Lett.* **1996**, *77*, 3865−3868.
(30) Zhang, H.; Xu, Z.; Chen, D.; Hu, B.; Zhou, Q.; Chen, S.; Li, S.; Sun, W.; Zhang, C. Adsorption mechanism of water molecules on hematite (104) surface and the hydration microstructure. *Appl. Surf. Sci.* **2021**, *550*, No. 149328.
(31) Cheng, Z.; Zhu, Y.; Li, Y.; Butt, S. Experimental and MD simulation of 3-dodecyloxypropanamine and 3-tetradecyloxypropylamine adsorbed onto quartz (101) surface. *Int. J. Min. Sci. Technol.* **2021**, *31*, 1033−1042.
(32) Qi, C.; Spagnoli, D.; Fourie, A. DFT-D study of single water adsorption on low-index surfaces of calcium silicate phases in cement. *Appl. Surf. Sci.* **2020**, *518*, No. 146255.
(33) Maslen, E. N.; Streltsov, V. A.; Streltsova, N. R.; Ishizawa, N.; Satow, Y. Synchrotron X-ray study of the electron density in alpha-Al2O3. *Acta Crystallogr., Sect. B: Struct. Sci.* **1993**, *49*, 973−980.
(34) Rath, S. S.; Sinha, N.; Sahoo, H.; Das, B.; Mishra, B. K. Molecular modeling studies of oleate adsorption on iron oxides. *Appl. Surf. Sci.* **2014**, *295*, 115−122.
(35) Noguera, C. Polar oxide surfaces. *J. Phys.: Condens. Matter* **2000**, *12*, R367−R410.
(36) Bandi, S.; Srivastav, A. K. Understanding the Growth Mechanism of Hematite Nanoparticles: The Role of Maghemite as an Intermediate Phase. *Cryst. Growth Des.* **2021**, *21*, 16−22.
(37) Catalano, J. G.; Fenter, P.; Park, C. Water ordering and surface relaxations at the hematite (110)-water interface. *Geochim. Cosmochim. Acta* **2009**, *73*, 2242−2251.
(38) Sun, L.; Zhan, W.; Li, Y.-A.; Wang, F.; Zhang, X.; Han, X. Understanding the facet-dependent catalytic performance of hematite microcrystals in a CO oxidation reaction. *Inorg. Chem. Front.* **2018**, *5*, 2332−2339.
(39) Meftah, Y.; Bekker, D.; Benhaoua, B.; Rahal, A.; Benhaoua, A.; Hamzaoui, A. H. Post annealing effect on structural and optical properties of (α-Fe2O3) thin films prepared by spray pyrolysis with moving nozzle. *Dig. J. Nanomater. Biostructures* **2018**, *13*, 465−474.
(40) Zhang, H.; Sun, W.; Zhang, C.; He, J.; Chen, D.; Zhu, Y. Adsorption performance and mechanism of the commonly used collectors with Oxygen-containing functional group on the ilmenite surface: A DFT study. *J. Mol. Liq.* **2022**, *346*, No. 117829.
(41) Qin, W.; Lin, C.; Cheng, W.; Xiao, X. Enhancing the Activity of Iron Based Oxygen Carrier via Surface Controlled Preparation for Lignite Chemical Looping Combustion. *Chem. J. Chin. Univ.* **2015**, *36*, 116−123.

https://doi.org/10.1021/acsomega.2c06101
ACS Omega 2023, 8, 8248−8255